Applied Catalysis B: Environmental 182 (2016) 115–122

Contents lists available at ScienceDirect

Applied Catalysis B: Environmental

journal homepage: www.elsevier.com/locate/apcatb

# Construction of high-dispersed Ag/$Fe_3O_4$/g-$C_3N_4$ photocatalyst by selective photo-deposition and improved photocatalytic activity

Zhi Zhu[a], Ziyang Lu[b], Dandan Wang[a], Xu Tang[a], Yongsheng Yan[a,*], Weidong Shi[a], Youshan Wang[a], Nailing Gao[a], Xin Yao[a], Hongjun Dong[a,*]

[a] School of Chemistry and Chemical Engineering, Jiangsu University, China
[b] School of the Environment and Safety Engineering, Jiangsu University, China

ARTICLE INFO

*Article history:*
Received 17 July 2015
Received in revised form
10 September 2015
Accepted 12 September 2015
Available online 14 September 2015

*Keywords:*
High-dispersed
Ag/$Fe_3O_4$/g-$C_3N_4$
Selective photo-deposition
Synergic effect
Photodegradation of tetracycline

ABSTRACT

A high-dispersed Ag/$Fe_3O_4$/g-$C_3N_4$ composite photocatalyst is firstly synthesized by means of the selective photo-deposition technique. It exhibits the obvious improvement of photocatalytic activity and stability for degrading tetracycline besides retaining the recycled magnetic property. The enhanced photocatalytic activity originates from synergetic effect of Ag, $Fe_3O_4$ and g-$C_3N_4$ that improves light absorption capacity and separation efficiency of charge carriers. This work provides a promising approach to develop visible-light-response and recycled photocatalysts applied to antibiotic wastewater treatment.


## 1. Introduction

In the course of the development of economy, some issues on environmental pollution emerged, which have restricted the sustainable development of modern human society [1,2]. The semiconductor photocatalytic technique, using the renewable solar energy to degrade organic pollutants to non-toxic products, has been interested by many researchers [3,4]. Therefore, exploiting the novel, high-efficient and eco-friendly photocatalysts are necessary for air purification and waste water treatment [5]. More recently, many semiconductors are used for degradation of organic pollutants, such as CdS, $TiO_2$, ZnO [6–8] etc. Among these semiconductors, graphite-like carbon nitride (g-$C_3N_4$) has drawn plenty of scientific interest [9–11] due to its potential application in solar energy conversion, such as poisonious gas treatment [12], water splitting [13,14], and photocatalytic degradation organic contaminant [15] under visible light irradiation. To date, the recent improvements of g-$C_3N_4$ have been published in a large number of articles. For example, the different morphologies of g-$C_3N_4$ were prepared successfully, such as three-dimensionally ordered macroporous g-$C_3N_4$, g-$C_3N_4$ quantum dots (QDs), and two-dimensionally ultrathin g-$C_3N_4$ nanosheets. Moreover, the g-$C_3N_4$ as photoelectronic materials makes it become a promising material to apply in photo-electrochemical anticorrosion, batteries, light emitting devices, fuel cells, solar cells, etc. However, there are still some disadvantages that restricted the application of g-$C_3N_4$ in environmental remediation [16], for example, the low surface area [17], high recombination rate of photogenerated electron–hole pairs, and the poor quantum yield [15,18]. Therefore, modification design of g-$C_3N_4$ for further widening visible light absorption and increasing stability is necessary to meet the requirement of practical environmental purification. In order to increase the photocatalytic performance of g-$C_3N_4$, the numerous methods have been employed, such as doping of metal/nonmetal elements [19,20], or coupling with other semiconductors [21,22]. However, all of these photocatalysts are notoriously difficult to recycle and even create huge waste.

Considering reduction of the raw materials waste, $Fe_3O_4$ nanoparticles have caused abroad attention owing to their high super-magnetism for easy separation by magnet, introduction into photocatalysts of which can effectively enhance the cyclic utilization rate [23,24]. The majority of researches have proven that $Fe_3O_4$/g-$C_3N_4$ not only could be recovered [25], but also showed good photocatalytic performance [26–28]. It is because $Fe_3O_4$ has the superior magnetism and a narrow band gap (0.1 eV) [29]. In gen-

* Corresponding authors. Fax: +86 511 8879 1800.
*E-mail addresses:* gchxz206@126.com (Y. Yan), donghongjun6698@aliyun.com (H. Dong).

http://dx.doi.org/10.1016/j.apcatb.2015.09.029
0926-3373/

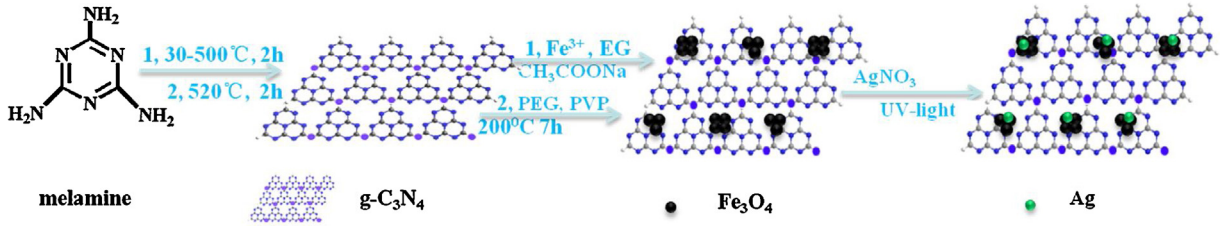


**Scheme 1.** Schematic preparation of $Ag/Fe_3O_4/g\text{-}C_3N_4$.

eral, $Fe_3O_4$ is similar to a conductor, due to its conductivity is as high as $1.9 \times 10^6\ Sm^{-1}$ [30] so that it can become the medium to transfer photogenerated electrons rapidly. Therefore, if we find a kind of materials to combine with $Fe_3O_4$, it will definitely more efficiently improve the separation efficiency of charge carriers. Noble metals loading may be a comparatively ideal method. Recently, coupling noble metal nanoparticles with semiconductors to facilitate charge separation has a large number of reports [31–33]. For example, by depositing Pt, Au and Ag nanoparticles onto semiconductor surface, it can improve the photocatalytic activity under visible light irradiation [34–36]. The possible reason is that the noble metals can strongly absorb visible light owing to their surface plasmon resonance effect (SPR) [37–39]. Ag nanoparticles are relative low-cost and widely used comparing with other noble metal, such as Ag@AgCl, Ag/AgX/GO and $Ag/g\text{-}C_3N_4$ etc., photocatalysts.

Inspired by above analyses, the $Ag/Fe_3O_4/g\text{-}C_3N_4$ composite photocatalyst is firstly prepared, in which Ag species selective deposit on the surface of $Fe_3O_4$ nanoclusters rather than $g\text{-}C_3N_4$. It not only exhibits improved photocatalytic activity than $Ag/g\text{-}C_3N_4$, $Fe_3O_4/g\text{-}C_3N_4$, and $g\text{-}C_3N_4$ for degrading tetracycline, but also shows high recycling rates. In addition, the optimization of experimental conditions and the mechanism of photocatalytic reaction are also systematically investigated.

## 2. Experimental

### 2.1. Materials

Melamine (99.0%), $CH_3COOHNa{\cdot}3H_2O$ (98.0%), NaOH (97%), Polyethylene glycol 1500 (PEG, 1500), ethylene glycol (98.0%) were all supported by Aladdin Chemistry Co., Ltd. $Fe(NO_3)_3{\cdot}9H_2O$ (98.0%), $AgNO_3$ (98.0%), ethanol ($C_2H_5OH$, 95.0%), Polyvinylpyrrolidone, (PVP) were purchased from Sinopharm Chemical Reagent Co., Ltd. Tetracycline was analytical pure and used without further purification, distilled water was used in the whole experiments.

### 2.2. Synthesis

The pure $g\text{-}C_3N_4$ was synthesized by annealing melamine in muffle. Briefly, 2.0 g melamine was put into an open crucible, heating to 500 °C from room temperature and holding for 2 h, then rising to 550 °C with a ramping rate of 2.3 °C $min^{-1}$ hold for another 2 h. After the alumina crucible cooled to room temperature, the as-prepared $g\text{-}C_3N_4$ was ground into powders, and underwent ultrasonic crashing 5 h. After the $g\text{-}C_3N_4$ was bathed in alkaline solution several hours, it continued roasting 2 h at 250 °C for further using.

$Fe_3O_4/g\text{-}C_3N_4$ was synthesized as follows: the as-prepared $g\text{-}C_3N_4$ (0.5 g) sample was added to ethanediol of 30 ml containing 0.25 g $Fe(NO_3)_3{\cdot}9H_2O$, 0.25 g $C_2H_3O_2Na{\cdot}3H_2O$, 0.03 g PEG, 0.005 g PVP, with ultrasonic dispersion 3 h. Then the suspension was transferred into a 50 ml teflonlined stainless steel autoclave after full dissolution and maintained the temperature of 200 °C for 10 h. After the product cooled to ambient temperature, it was washed with deionized water and ethanol for several times. $Ag/Fe_3O_4/g\text{-}C_3N_4$ was synthesized as follows: Appropriate amount of $AgNO_3$ and $Fe_3O_4/g\text{-}C_3N_4$ were added to distilled water of 30 ml in beaker. The suspension was stirred under the irradiation of an UV-lamp for 10 min. After completion of the reaction, the suspension was separated by magnet. Subsequently, the precipitate was washed by deionized water and ethanol for several times, and transferred to oven to dry at 80 °C. the preparation process of $Ag/Fe_3O_4/g\text{-}C_3N_4$ is shown in Scheme 1.

### 2.3. Characterization

X-ray diffraction patterns (XRD) of the samples recorded at room temperature, and the patterns of the photocatalyst were obtained with a D/max-RA X-ray diffractometer (Rigaku, Japan) which equipped with Ni-filtrated Cu K*a* radiation (40 kV, 200 mA) at 5–80° with a scanning step of 0.02°/0.2 s. The infrared spectra were obtained on a Nicolet Magna-IR 550 Fourier transform infrared (FT-IR) spectrometer and KBr as the reference sample within wavelength range of 400–4000 $cm^{-1}$. Raman experiments were performed using a DXR spectrometer using the 532 nm laser, and measurements were made in backscattering geometry. The transmission electron microscope (TEM) images were examined with JEM-2100 transmission electron microscopy (JEOL, Japan). The magnetic was carried out by using a vibrating sample magnetometer (VSM) (HH-15, Jiangsu University). Inductively coupled plasma optical emission spectrometry (ICP-OES, VISTA-MPX) was designed to analyze chemical composition of photocatalysts. The room-temperature photoluminescence (PL) spectra of $g\text{-}C_3N_4$, $Fe_3O_4/g\text{-}C_3N_4$ and $Ag/Fe_3O_4/g\text{-}C_3N_4$ were investigated utilizing the (Cary Eclipse Spectrophotometer, VARIAN, USA) equipped with xenon (Xe) lamp with an excitation wavelength of 345 nm. UV–vis diffuse reflectance spectra (DRS) were obtained using a Shimadzu UV-3600 spectrometer by using $BaSO_4$ as a reference.

### 2.4. Adsorption experiments

For investigating the adsorption capability of phtocatalysts, the adsorption experiments were as below. 0.05 g photocatalyst was added into photocatalytic reactor containing 20 mg $L^{-1}$ tetracycline solutions (100 ml). 8 ml solutions were sampled with an injector in each 15 min after stirring for 70 min in the dark at 25 °C, the solution was filtered and the concentration of tetracycline was determined with UV–vis spectroscopy at a wavelength of 357 nm.

### 2.5. Photocatalytic experiments

The photocatalytic activities were evaluated through decomposing tetracycline under visible light irradiation (a 300 W Xe lamp with a 420 nm cut off filter). 0.05 g photocatalyst was totally suspended in an aqueous solution of tetracycline (100 ml, 20 mg $L^{-1}$). Before irradiation, the suspensions were magnetically stirred in dark for 50 min to get absorption–desorption equilibrium between the photocatalyst and tetracycline. At irradiation time interval of

every 15 min, 8 ml solution was sampled and magnetic separated, then monitoring the absorbance of tetracycline.

Moreover, the experiments of radicals capture were carried out by adding 1 mmol triethanolamine (OA, a quencher of $h^+$), 1 mmol isopropanol (IPA, a quencher of $^{\bullet}OH$), and 1 mmol benzoquinone (BQ, a quencher of $^{\bullet}O_2^-$), respectively. The concentration of tetracycline in solution was determined by spectrophotometer. The photocatalytic efficiency was calculated according to $\eta = (C_0 - C_t)/C_0$, where $\eta$ is the photocatalytic efficiency; $C_0$ is the concentration of reactant before illumination; $C_t$ is the concentration of reactant after illumination time.

### 2.6. Photoelectrochemical (PEC) measurement

The corresponding electrodes were prepared as follows: the as-prepared photocatalyst of 0.1 g was dispersed in 1.0 ml ethanol, then adding 1.0 ml ethanol glycol. The above mixture was dip-coated onto a $1 \times 1\ cm^2$ fluorine-doped tin oxide glass electrode, and then calcined in air at 80 °C for 1 h. The PEC measurements were carried out in a conventional three-electrode. Single-compartment quartz cell filled with 0.5 M $Na_2SO_4$ electrolyte. The working electrodes are Ag/$Fe_3O_4$/g-$C_3N_4$ thin films. The platinum wire electrode and the Ag/AgCl electrode were used as counter electrode and reference electrode, respectively. The illumination source is a 300 W Xe lamp (PLS-SXE300 (UV), Perfect light Technology Co., Ltd., Beijing). The distance of illumination source and the photoelectrode was fixed to be 20 cm. The PEC measurements were performed on a CHI 760D electrochemical analyzer (ChenHua Instruments, Shanghai, China).

## 3. Results and discussion

### 3.1. Characterization of the samples

XRD pattern is used to investigate the phase structures of the samples. Fig. 1a shows the typical diffraction patterns of pure g-$C_3N_4$. The peak at 27.4° is due to the stacking of the conjugated aromatic system, which is indexed for graphitic materials as the (0 0 2) peak of g-$C_3N_4$ [40]. Fig. 1b displays XRD pattern of $Fe_3O_4$/g-$C_3N_4$, where the peaks of $Fe_3O_4$ crystal phase at $2\theta = 30.2°$, 35.5°, 43.2°, 53.4°, 57.3° and 62.6° can be found [41]. It is worth noting that the diffraction peak positions at 27.4° in Fig. 1b is slightly lower, which may result from restraining the stacking of g-$C_3N_4$ perpendicular to the [0 0 2] direction owing to introducing $Fe_3O_4$. It is in favor of increasing dispersity and specific surface area of g-$C_3N_4$, thus improving photocatalytic performance. Furthermore, the diffraction patterns of Ag/$Fe_3O_4$/g-$C_3N_4$ were performed and shown in Fig. 1c–g. The characteristic diffraction peaks of Ag at $2\theta = 38.0°$, 44.2°, 64.4° and 77.4° were found obviously, which indicates the formation of Ag/$Fe_3O_4$/g-$C_3N_4$ ternary composites. It is interesting that the peak intensity of Ag (38.0°) become stronger gradually with its contents increasing; in contrast, the peak intensity of $Fe_3O_4$ (35.5°) become weaker and weaker [42]. This implies that Ag species may deposit on the surface of $Fe_3O_4$ nanoclusters rather than g-$C_3N_4$ because the diffraction peak (0 0 2) of g-$C_3N_4$ has hardly changed with Ag contents increasing.

Fig. 2 shows the FT-IR spectra of g-$C_3N_4$, $Fe_3O_4$/g-$C_3N_4$, and Ag/$Fe_3O_4$/g-$C_3N_4$. For pure g-$C_3N_4$, a series absorption peaks are observed in Fig. 5a. The broad absorption peaks from 3400 $cm^{-1}$ to 3000 $cm^{-1}$ are assigned to the stretching vibrational modes of primary (=NH) and secondary (—NH) amines. The peaks at 1251 $cm^{-1}$, 1325 $cm^{-1}$, 1419 $cm^{-1}$, 1575 $cm^{-1}$, and 1639 $cm^{-1}$ correspond to the typical stretching modes of the CN heterocycles [43]. Additionally, the characteristic breathing mode at 808 $cm^{-1}$ is attributed to the typical bending vibration of *s*-triazine units [44]. As shown in

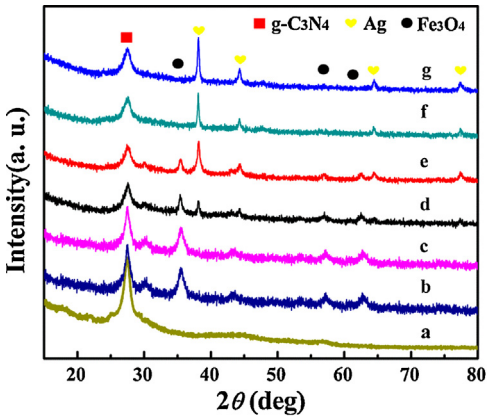


**Fig. 1.** XRD patterns of pure g-$C_3N_4$ (a), $Fe_3O_4$/g-$C_3N_4$ (b), Ag/$Fe_3O_4$/g-$C_3N_4$ with different Ag content, 0.5 wt.% (c), 1.5 wt.% (d), 3.0 wt.% (e), 5.0 wt.% (f), and 7.0 wt.% (g).

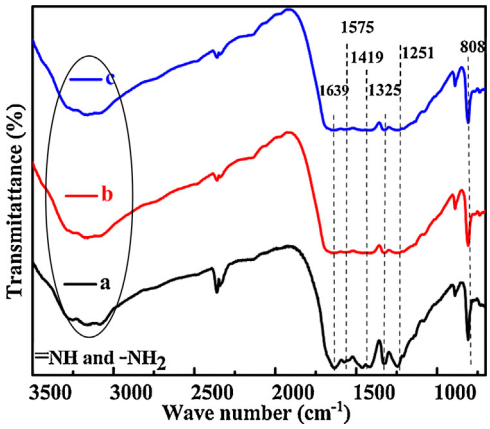


**Fig. 2.** FT-IR spectra of pure g-$C_3N_4$ (a), $Fe_3O_4$/g-$C_3N_4$ (b), and Ag/$Fe_3O_4$/g-$C_3N_4$ (c).

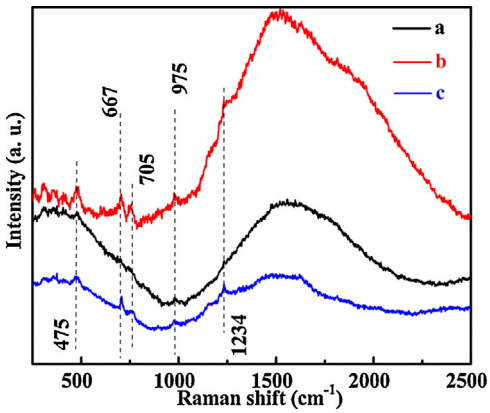


**Fig. 3.** Raman spectra of g-$C_3N_4$ (a), $Fe_3O_4$/g-$C_3N_4$ (b), Ag/$Fe_3O_4$/g-$C_3N_4$ (c).

Fig. 4b, the FT-IR spectrum of $Fe_3O_4$/g-$C_3N_4$ exhibits the absorption peaks of g-$C_3N_4$ become slight weaker, which illustrates hydrothermal treatment has no effect on the chemical structure of g-$C_3N_4$. Compared with Fig. 2b, the absorption peaks of Ag/$Fe_3O_4$/g-$C_3N_4$ in Fig. 2c are almost no change after depositing Ag nanoparticles, which proves indirectly that Ag species deposit selectively on the $Fe_3O_4$ nanocluster surface, in accordance with XRD results.

Raman spectroscopy is usually used to research the vibrational properties of carbon materials. From the Raman spectrum of pure g-$C_3N_4$ in Fig. 3a, the peaks located at 475 $cm^{-1}$, 705 $cm^{-1}$, 974 $cm^{-1}$, and 1234 $cm^{-1}$ stem from the vibration modes of CN heterocycles

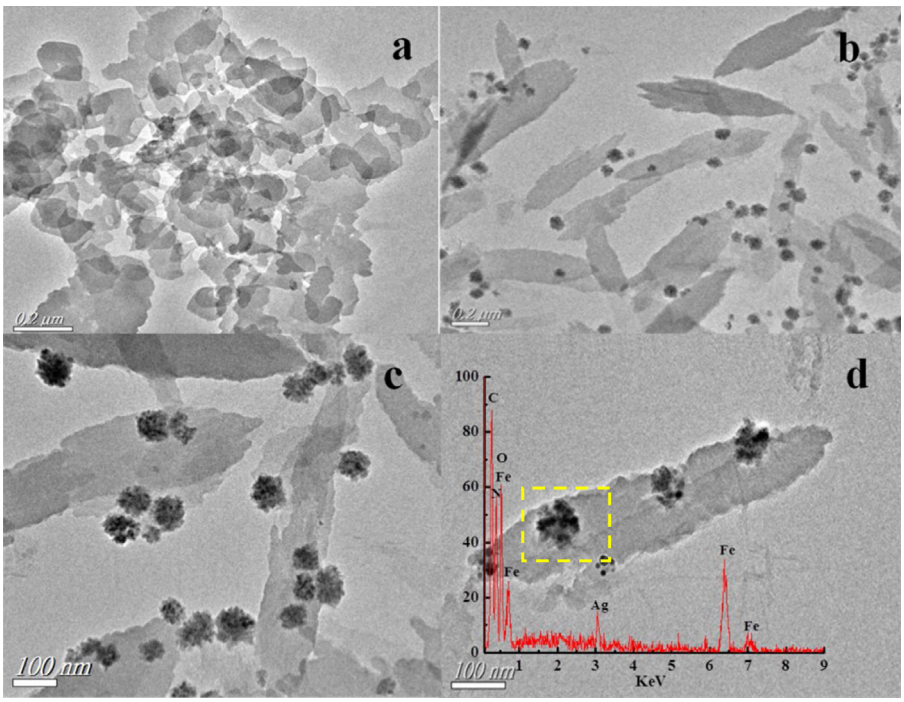


**Fig. 4.** TEM images of g-$C_3N_4$ (a), $Fe_3O_4$/g-$C_3N_4$ (b) and Ag/$Fe_3O_4$/g-$C_3N_4$ (c), single amplified Ag/$Fe_3O_4$/g-$C_3N_4$ (d) and the EDX of single amplified Ag/$Fe_3O_4$/g-$C_3N_4$ (the insert of d).

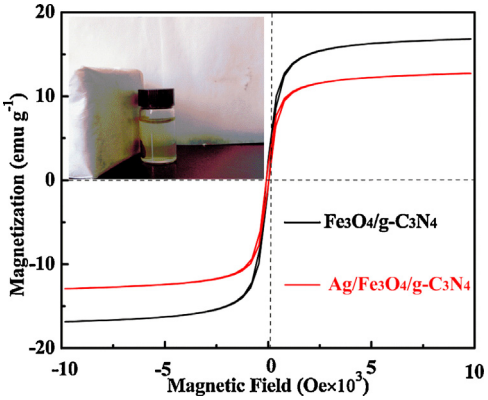


**Fig. 5.** Hysteresis loops of $Fe_3O_4$/g-$C_3N_4$ and Ag/$Fe_3O_4$/g-$C_3N_4$ under magnetic field.

in g-$C_3N_4$ [45,46]. In addition, besides the mentioned peaks of pure g-$C_3N_4$ in Raman spectrum of $Fe_3O_4$/g-$C_3N_4$ (Fig. 3b), one prominent peak bond occurs at 667 $cm^{-1}$ that is symmetric stretch of oxygen atoms along Fe—O bond [47], which indicates that $Fe_3O_4$ successfully grows on the g-$C_3N_4$ surface. Interestingly, the peak coming from Fe—O bond is weakened significantly in the Raman spectrum of Ag/$Fe_3O_4$/g-$C_3N_4$ (Fig. 3c), which further demonstrates Ag species covering on $Fe_3O_4$ surface once again.

The morphology and formation of Ag/$Fe_3O_4$/g-$C_3N_4$ composites are further investigated by TEM. It can be seen that the pure g-$C_3N_4$ sample displays irregular thin sheet and overlapping together obviously (Fig. 4a). In contrast, after hydrothermal reaction process of 10 h, the morphology of $Fe_3O_4$/g-$C_3N_4$ sample exhibits regular uniform bamboo leaves-like shape with the size of 0.5–0.8 μm, possessing high-degree dispersity (Fig. 4b). Meanwhile, the $Fe_3O_4$ nanoclusters with an average diameter of 50–80 nm uniformly deposit on the surface of g-$C_3N_4$ at the hydrothermal reaction. Moreover, when Ag depositing, there are not obviously morphology changes of Ag/$Fe_3O_4$/g-$C_3N_4$ (Fig. 4c) compared with that of $Fe_3O_4$/g-$C_3N_4$. It is noteworthy that there are some smaller nanoparticles observed on the surface of $Fe_3O_4$ rather than g-$C_3N_4$ (Fig. 4d). By means of performing EDX spectroscopy analyses of $Fe_3O_4$ nanoclusters region on the Ag/$Fe_3O_4$/g-$C_3N_4$ sample (the insert of Fig. 4d), Fe, O, Ag, C and N elements are clearly detected out, which indicates the Ag species selectively deposit on the surface of $Fe_3O_4$ combining with the results of XRD patterns, FT-IR spectra and Raman spectra.

**Table 1**
The composition of Ag and $Fe_3O_4$ in $Fe_3O_4$/g-$C_3N_4$ and Ag/$Fe_3O_4$/g-$C_3N_4$.

| Photocatalyst | $Fe_3O_4$ (%) | Ag (%) |
|---|---|---|
| $Fe_3O_4$/g-$C_3N_4$ | 8.89 | – |
| Ag/$Fe_3O_4$/g-$C_3N_4$ | 8.68 | 2.87 |

The magnetic property is measured by the applied field sweeping from 10 to 10000 kOe at room temperature. Fig. 5 shows that the $Fe_3O_4$/g-$C_3N_4$ exhibits distinctly a symmetric hysteresis loop, and its magnetization saturation (Ms) value reaches to 16.80 emu $g^{-1}$. In comparison, the magnetization saturation (Ms) value of Ag/$Fe_3O_4$/g-$C_3N_4$ is slightly lower than that of $Fe_3O_4$/g-$C_3N_4$ (12.68 emu $g^{-1}$). This magnetism reduction of Ag/$Fe_3O_4$/g-$C_3N_4$ may be caused by the introduction of Ag species on the surface of $Fe_3O_4$. However, the photo (the inset of Fig. 5d) displays that the dispersed suspension becomes clearly and transparent, which demonstrates that Ag/$Fe_3O_4$/g-$C_3N_4$ is still easily separated by a magnet, possessing the outstanding magnetic separation performance.

As we known that ICP-AES is one of the effective detection technique for most metal elements, which is used to identify the contents of Fe and Ag in the sample. The results are shown in Table 1. The contents of $Fe_3O_4$ and Ag in Ag/$Fe_3O_4$/g-$C_3N_4$ sample are 8.68 wt.% and 2.87 wt.%, respectively, which are close to the experimental designed values ($Fe_3O_4$ 9.0 wt.% and Ag 3.0 wt.%). Remarkably, the content of $Fe_3O_4$ in Ag/$Fe_3O_4$/g-$C_3N_4$ is similar to that of $Fe_3O_4$/g-$C_3N_4$ (8.89 wt.%). It implies that the enhanced preformance of Ag/$Fe_3O_4$/g-$C_3N_4$ mainly attributes to the introducting Ag speices and has nothing to do with content of $Fe_3O_4$.

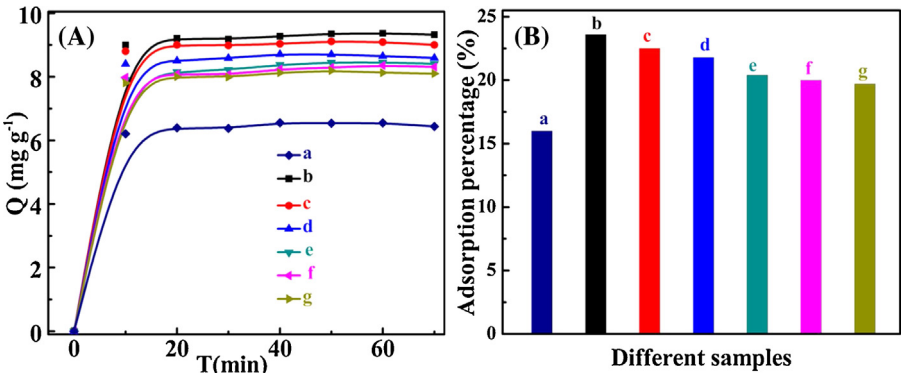


**Fig. 6.** Adsorption curves (A) and adsorption percentage (B) of tetracycline molecules over the different samples:pure g-$C_3N_4$ (a), $Fe_3O_4$/g-$C_3N_4$ (b), Ag/$Fe_3O_4$/g-$C_3N_4$ with different Ag content, 0.5 wt.% (c), 1.5 wt.% (d), 3.0 wt.% (e), 5.0 wt.% (f), and 7.0 wt.% (g).

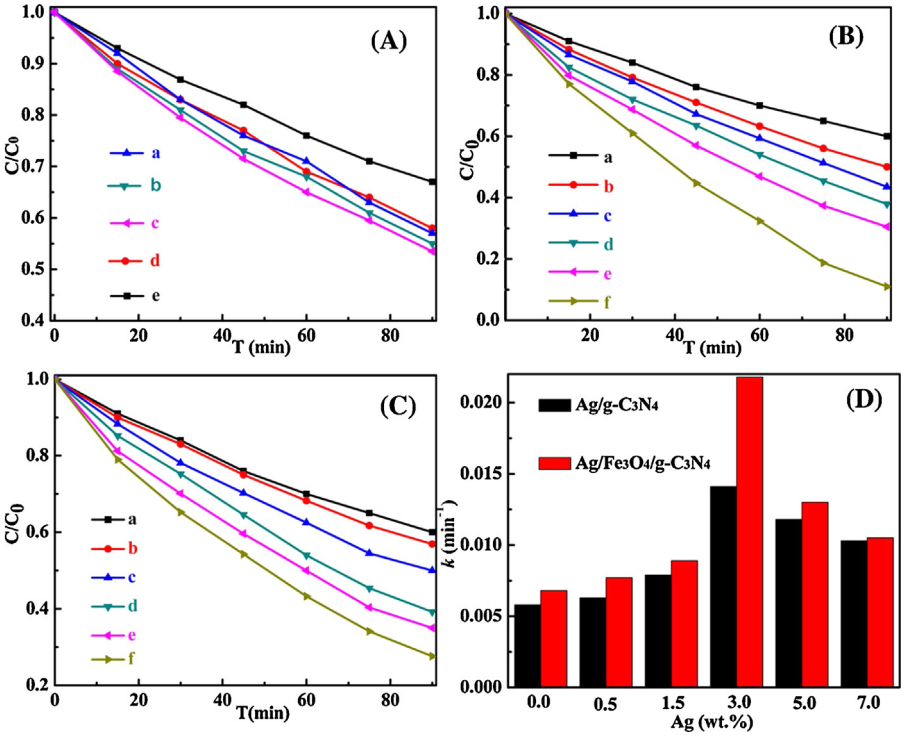


**Fig. 7.** Degradation dynamics curves of tetracycline over different samples under visible light irradiation (A–C): (A) $Fe_3O_4$/g-$C_3N_4$ with different $Fe_3O_4$ content, 1.0 wt.% (a), 6.0 wt.%/g-$C_3N_4$ (b), 9.0 wt.% (c), 12.0 wt.% (d), 20.0 wt.% (e). (B) Ag/$Fe_3O_4$/g-$C_3N_4$ with different Ag content, $Fe_3O_4$/g-$C_3N_4$ (a), 0.5 wt.% (b), 1.5 wt.% (c), 3.0 wt.% (d), 5.0 wt.% (e), and 7.0.wt% (f). (C) Ag/g-$C_3N_4$ with different Ag content, pure g-$C_3N_4$ (a), 0.5 wt.% (b), 1.5 wt.% (c), 3.0 wt.% (d), 5.0 wt.% (e), and 7.0 wt.% (f). (D) The first-kinetic constant *k* of Ag/g-$C_3N_4$ and Ag/$Fe_3O_4$/g-$C_3N_4$ with different Ag (wt.%) contents.

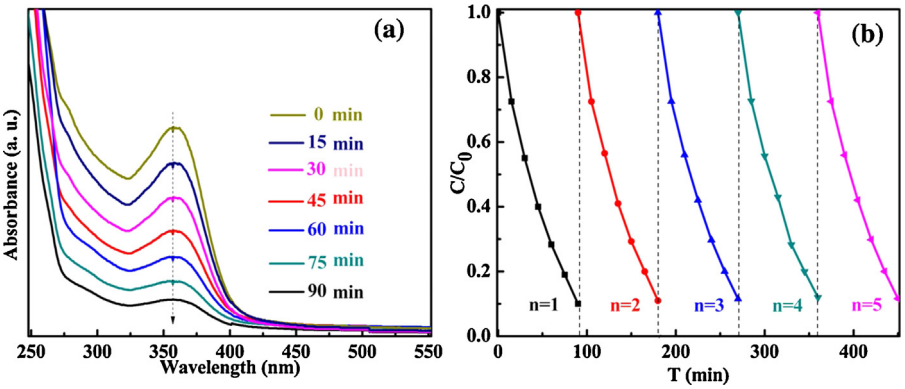


**Fig. 8.** Time-dependent absorption spectra of tetracycline solution (a), and the cycling runs in the photocatalytic degradation of tetracycline (b) over Ag/$Fe_3O_4$/g-$C_3N_4$.

### 3.2. Adsorption capacity

Fig. 6a is the absorption curves of tetracycline molecules over the different samples, which shows the solution systems almost reached adsorption equilibrium in the time of 40 min. It is obvious that $Fe_3O_4$/g-$C_3N_4$ has the highest adsorption capacity that reaches to 9.0 mg $g^{-1}$, which may be attributed to the electrostatic stabilization of the $Fe_3O_4$ nanocluster to tetracycline molecules owing to the main interaction attraction existed between the $Fe_3O_4$ and tetracycline molecules [48,49]. Moreover, the adsorption capacity of Ag/$Fe_3O_4$/g-$C_3N_4$ reduces gradually with increasing Ag contents compared with $Fe_3O_4$/g-$C_3N_4$ (from 7.8 mg $g^{-1}$ to 8.9 mg $g^{-1}$), which may result from the covering effect of Ag species on the adsorption sites of $Fe_3O_4$, but it is still much higher than that of pure g-$C_3N_4$ (6.1 mg $g^{-1}$). The results are further exhibited directly by the adsorption percentage of different samples in Fig. 6B. The superior adsorption capacity is in favor of improving photocatalytic activity because of the full contact between target molecules and photocatalyst. We should point out that Ag/$Fe_3O_4$/g-$C_3N_4$ with slight lower adsorption capacity exhibits the higher photocatalytic activity than that of $Fe_3O_4$/g-$C_3N_4$, which also indirectly testifies that the introduction of Ag species play important role for enhancing photocatalytic performance.

### 3.3. Photocatalytic activity

The photocatalytic activities of as-prepared samples are evaluated by the degradation of antibiotics under visible light irradiation. Firstly, the optimizing content of $Fe_3O_4$ in $Fe_3O_4$/g-$C_3N_4$ is obtained. From degradation dynamics curves of tetracycline over the $Fe_3O_4$/g-$C_3N_4$ samples with different content of $Fe_3O_4$ in Fig. 7A, when the percentage of $Fe_3O_4$ is 9.0 wt.%, $Fe_3O_4$/g-$C_3N_4$ exhibits the highest photocatalytic activity. Moreover, the photodegradation activity of Ag/$Fe_3O_4$/g-$C_3N_4$ containing different amount of Ag is further investigated. As shown in Fig. 7B, after the surface of $Fe_3O_4$ is selectively modified by Ag species, photocatalytic activity of Ag/$Fe_3O_4$/g-$C_3N_4$ for removing tetracycline molecules is distinctly enhanced. When the content of Ag species increases to 3.0 wt.%, the photocatalytic activity of Ag/$Fe_3O_4$/g-$C_3N_4$ is optimal and degradation rate of tetracycline reaches to 88% undergoing photocatalytic reaction of 90 min. In addition, the excess Ag species will lead to the reduction of photocatalytic activity owing to the shielding effect that weakens light harvest of Ag/$Fe_3O_4$/g-$C_3N_4$. We have point out that the formation of heterojunction between $Fe_3O_4$ and g-$C_3N_4$ is a major reason for enhancing photocatalytic activity owing to improving separation efficiency of charge carriers. Especially for introduction of Ag species, Ag nanoparticles selectively deposited on the surface of $Fe_3O_4$ not only induce plasmon resonance effect to widen light absorption ability, but also can export photogenerated electrons on the $Fe_3O_4$/g-$C_3N_4$, which more efficiently improves the separated ability of electron–hole pairs, thus resulting in the higher photocatalytic activity. Meanwhile, the photocatalytic activity of Ag/g-$C_3N_4$ prepared by means of Ag species directly depositing on the surface of g-$C_3N_4$ is evaluated under visible light. From the degradation dynamics curves of tetracycline over Ag/g-$C_3N_4$ with different amount of Ag in Fig. 7C, we find that Ag/g-$C_3N_4$ containing 3.0 wt.% Ag exhibit the highest photocatalytic activity. In order to compare explicitly the photocatalytic activity between Ag/$Fe_3O_4$/g-$C_3N_4$ and Ag/g-$C_3N_4$, the rate constants are all calculated according to pseudo-first-order reaction equation by plotting ln ($C0/C$)~$t$. Fig. 7D presents the comparison of rate constants of Ag/$Fe_3O_4$/g-$C_3N_4$ and Ag/g-$C_3N_4$ with the same Ag contents. It obviously shows that the rate constants of Ag/$Fe_3O_4$/g-$C_3N_4$ are all higher than that of Ag/g-$C_3N_4$ at the same Ag content conditions. The maximal rate constant of Ag/$Fe_3O_4$/g-$C_3N_4$ reaches to 0.0218 $min^{-1}$, which is 1.55 times higher than that of Ag/g-$C_3N_4$ (0.0141 $min^{-1}$). All above results indicate that the constructed Ag/$Fe_3O_4$/g-$C_3N_4$ ternary composite photocatalyst has more intense photocatalytic activity for degrading tetracycline than that of $Fe_3O_4$/g-$C_3N_4$, Ag/g-$C_3N_4$ and g-$C_3N_4$. It implies that the synergistic effect existed between Ag, $Fe_3O_4$, and g-$C_3N_4$ should play an important role in preventing direct recombination of electron–hole pairs, thus improving photocatalytic activity.

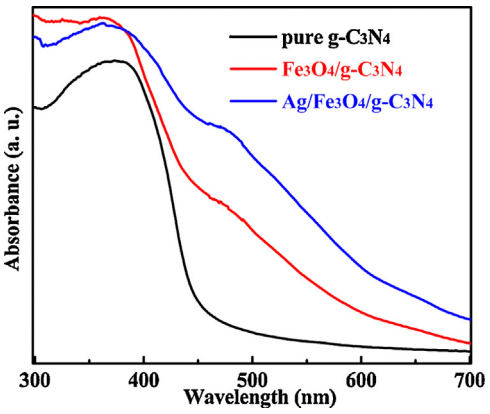


**Fig. 9.** UV–vis diffuse reflectance spectra of pure g-$C_3N_4$, $Fe_3O_4$/g-$C_3N_4$ and Ag/$Fe_3O_4$/g-$C_3N_4$.

In addition, the absorbance variations of tetracycline over Ag/$Fe_3O_4$/g-$C_3N_4$ are also performed. Fig. 8a illustrates that the absorbance of tetracycline decreases obviously with increase of light irradiation time. No absorbance peak is observed after visible light irradiation of 90 min, which indirectly proved that the tetracycline molecules are destroyed or decomposed into small molecules completely [50,51]. Furthermore, for the photocatalysts, the durability and stability was also crucially important for their practical applications. The recycling capability of Ag/$Fe_3O_4$/g-$C_3N_4$ is verified by carrying out a five-run test for degradation of tetracycline. As displayed in Fig. 8b, it reveals that the degradation rate has no obvious decrease after the five-run test, which illustrates that Ag/$Fe_3O_4$/g-$C_3N_4$ has the satisfactory reusability.

The photocatalytic activity of the photocatalysts is closely related to their light absorption ability. For comparison, the UV–vis DRS of pure g-$C_3N_4$, $Fe_3O_4$/g-$C_3N_4$, and Ag/$Fe_3O_4$/g-$C_3N_4$ are measured and shown in Fig. 9. It is clear that g-$C_3N_4$ shows absorption wavelengths from the UV to the visible range up to 460 nm (Fig. 9a) and its band gap is ~2.7 eV (the insert of Fig. 9) that agrees well with the previous reports [52,53]. In comparisons, Fig. 9b shows that $Fe_3O_4$/g-$C_3N_4$ displays the more intense light absorption ability and its light harvest range also exhibits obvious red-shift reaching to ~700 nm, which are mainly result from the narrower band gap of $Fe_3O_4$. Furthermore, when the Ag species are selectively deposited on the surface of $Fe_3O_4$, Ag/$Fe_3O_4$/g-$C_3N_4$ presents more intense light absorption in the visible light region form 400 nm–700 nm. And there is an absorption peak ranged from 460 $cm^{-1}$ to 490 $cm^{-1}$, this may be attributed to the surface plasmon resonance (SPR) effect of Ag species [54]. The wider light adsorption region of the Ag/$Fe_3O_4$/g-$C_3N_4$ is able to make the most of visible light and produce more effectively photogenerated charge carriers, resulting in the higher photocatalytic activity.

The transfer and recombination process of electron–hole pairs in the interfaces of composite photocatalysts is one of most important effect factor on photocatalysis activity. The efficient separation of charge carriers can enhance the photocatalytic performance of photocatalyst. As well known that photoluminescence (PL) spectrum is widely used to investigate the migration, transfer and recombination of electron–hole pairs [55,56]. The PL spectra of the g-$C_3N_4$,

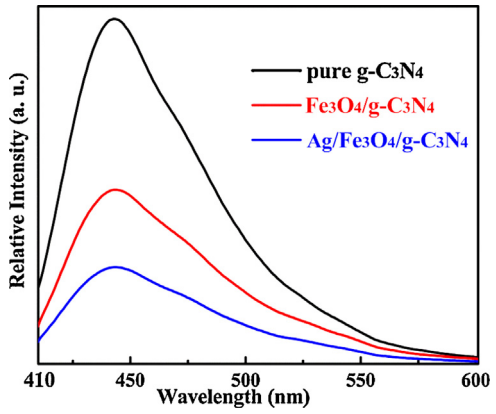


**Fig. 10.** Photoluminescence (PL) spectra of pure g-$C_3N_4$, $Fe_3O_4$/g-$C_3N_4$ and Ag/$Fe_3O_4$/g-$C_3N_4$.

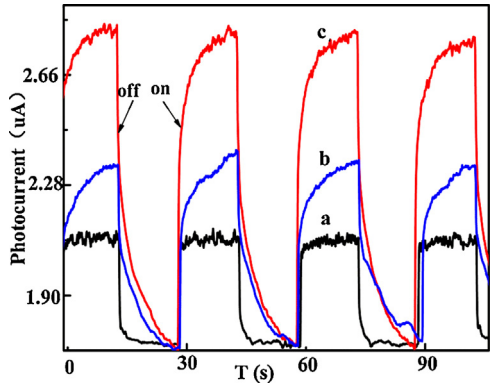


**Fig. 11.** Photocurrent response curves of g-$C_3N_4$ (a), $Fe_3O_4$/g-$C_3N_4$ (b), Ag/$Fe_3O_4$/g-$C_3N_4$ (c) under visible light irradiation.

$Fe_3O_4$/g-$C_3N_4$ and Ag/$Fe_3O_4$/g-$C_3N_4$ samples are shown in Fig. 10. It can be observed that g-$C_3N_4$ displays more intense fluorescence emission peak at ~435 nm, while the PL intensity of $Fe_3O_4$/g-$C_3N_4$ is distinct lower than that of it. The lower PL intensity is necessarily linked with the good electrical conductivity of $Fe_3O_4$, which implies the efficient interfacial electron transfer from conduction band of g-$C_3N_4$ to that of $Fe_3O_4$ nanoclusters, hampering the recombination of photoinduced charge carriers. Moreover, the PL spectrum of Ag/$Fe_3O_4$/g-$C_3N_4$ is further taking place more seriously quenching phenomenon compared with $Fe_3O_4$/g-$C_3N_4$, which should relate to good electrical conductivity and induced SPR effect of Ag species. Therefore, Ag/$Fe_3O_4$/g-$C_3N_4$ inhibits more effectively the recombination of photogenerated charge carriers to improve photocatalytic activity.

To further understand the separation and recombination of electron–hole pairs in the composite photocatalysts, the photocurrent test is also carried out under visible light. Generally, the corresponding relationship is that the higher the photocurrent implies the higher electrons–holes separation efficiency, thus leading to the higher the photocatalytic activity [57]. Fig. 11 shows the photocurrent-time curves under the dark and visible light in an on-and-off cycle mode. Obviously, the Ag/$Fe_3O_4$/g-$C_3N_4$ presents the highest photocurrent response intensity than $Fe_3O_4$/g-$C_3N_4$ and g-$C_3N_4$, which indicates that it has the lowest electrons and holes recombination rate. This give further an evidence to support the above PL results.

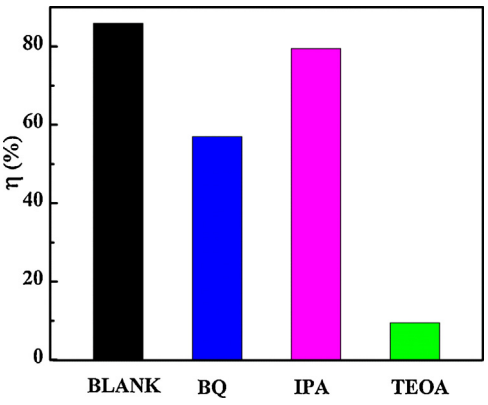


**Fig. 12.** Photodegradation rates of tetracycline over Ag/$Fe_3O_4$/g-$C_3N_4$ in the present of different scavengers.

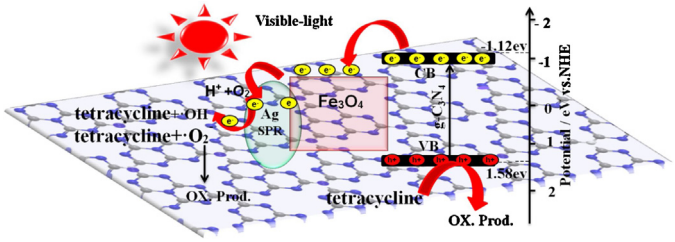


**Fig. 13.** Schematic illustration of the mechanism for photogenerated charge carrier transfers in the Ag/$Fe_3O_4$/g-$C_3N_4$ under visible light irradiation.

### 3.4. Photocatalytic mechanism

For purpose of in-depth investigating photodegradation mechanism of tetracycline, a variety of experiments are performed. The radical capture experiment is an effective method to investigate photodegradation reaction pathways of organic molecules on the surface of photocatalyst, because the interaction between the capturer and photocatalyst plays a dominant role for impacting on degradation efficiency of organic molecules. Generally, superoxide radicals ($^{\bullet}O_2^-$), hydroxyl radicals ($^{\bullet}OH$) and photogenerated holes are the acknowledged activated species in the photocatalytic degradation of organic pollutants. Therefore, a serious of radicals trapping experiments were performed by using of IPA (a quencher of $^{\bullet}OH$), BQ (a quencher of $^{\bullet}O_2^-$), TEOA (a quencher of $h^+$) over the Ag/$Fe_3O_4$/g-$C_3N_4$ sample [58–60]. As can be seen from the dynamic curves of tetracycline degradation over the Ag/$Fe_3O_4$/g-$C_3N_4$ sample under the visible-light in Fig. 12, it can be found that the photodegradation rate of tetracycline still reaches to ~79% in the presence of IPA, which is slightly lower than that of without any trapping agents (~88%). It implies that hydroxyl radicals ($^{\bullet}OH$) has almost no effect on photodegradation of tetracycline. On the contrary, when the TEOA and BQ are used, the photodegradation rates of tetracycline are distinctly reduction, and are only ~10% and ~58%, respectively, which indicates holes ($h^+$) and superoxide radicals $^{\bullet}O_2^-$ are main activated species. Thus, the influence order of the activated species in the process of tetracycline photodegradation is $h^+ > {}^{\bullet}O_2^- > {}^{\bullet}OH$.

As described in Fig. 13, The Schematic illustration shows the electron–hole separation processes and photodegradation mechanism of tetracycline. Firstly, when Ag/$Fe_3O_4$/g-$C_3N_4$ is exposed to visible-light, the g-$C_3N_4$ produced electrons and holes (Eq. (1)). The electrons on conduction band of the g-$C_3N_4$ rapidly transfer to $Fe_3O_4$, and further transfer to Ag ($Fe_3O_4$ surface) because of the good electrical conductivity of $Fe_3O_4$ and the electron storing capacity of Ag nanoparticles [61]. Therefore, a part of photoelec-

trons on g-$C_3N_4$ conduction band by $Fe_3O_4$ transfer indirectly to Ag nanoparticles served as terminal electron acceptor, thus prolonging the photogenerated electrons lifetime and facilitating the charge separation in the whole photocatalytic system. This result has been confirmed by the PL spectra and photocurrent test. On this account, the interfacial electrons transfer processes are effectively achieved. Secondly, the photogenerated electrons react with $O_2$ absorbed on the surface of Ag particles to produce the active species $^{\bullet}O_2^-$ (Eq. (2)), then $^{\bullet}O_2^-$ may also react with $H^+$ to further produce $^{\bullet}OH$ (Eq. (3)). Both $^{\bullet}O_2^-$ and $^{\bullet}OH$ all can oxidize tetracycline (Eqs. (4) and (5)). At the same time, the holes from g-$C_3N_4$ can also directly oxidize tetracycline (Eq. (6)). In addition, according to the previous reports, the holes on g-$C_3N_4$ surface cannot react with $H_2O$ and $OH^-$ to form $^{\bullet}OH$, which may be due to the g-$C_3N_4$ valence band (+1.57 eV) possessing more negative than $^{\bullet}OH/OH^-$ (+1.99 eV) [49]. It is the reason of the lowest content of $^{\bullet}OH$. Based on the above analysis, the charge carrier transfers and degradation reactions are proposed as follows:

$$g - C_3N_4 + h\upsilon \rightarrow g - C_3N_4\left(e^- + h^+\right) \quad (1)$$

$$O_2 + e^- \rightarrow {}^{\bullet}O_2^- \quad (2)$$

$$^{\bullet}O_2^- + 2H^+ \rightarrow 2{}^{\circ}OH \quad (3)$$

$$^{\bullet}O_2^- + \text{tetracycline} \rightarrow \text{OX. Pord.} \quad (4)$$

$$^{\circ}OH + \text{tetracycline} \rightarrow \text{OX. Pord.} \quad (5)$$

$$h^+ + \text{tetracycline} \rightarrow \text{OX. Pord.} \quad (6)$$

## 4. Conclusions

In summary, the high-dispersed Ag/$Fe_3O_4$/g-$C_3N_4$ composite photocatalyst is successfully prepared, whose optimal amounts of $Fe_3O_4$ and Ag are obtained and investigated in detail. This technique of selective Ag photo-depositing on the surface of $Fe_3O_4$ not only retains the recycled magnetic property, but also improves photocatalytic activity and stability for degradation of tetracycline. The enhanced photocatalytic activity is closely associated with electrons trapping of $Fe_3O_4$ nanoclusters and final electrons transferring to Ag species, which leads to the more intense light harvest and higher separation efficiency of electron–hole pairs. The synergetic mechanism of Ag, $Fe_3O_4$ and g-$C_3N_4$ that improves photocatalytic activity is distinctly confirmed by photoluminescence (PL) properties, photocurrent responses, and active species trapping experiments. The present study provides a promising photocatalytic material for removing antibiotic pollutants.

## Acknowledgements

This work was financially supported by the National Natural Science Foundation of China (Nos. 21306068 and 21407059), the Natural Science Foundation of Jiangsu Province (Nos. BK20130477, BK20130480,BK20130487 and BK20140527), the China Postdoctoral Science Foundation (Nos. 2012M521015 and 2014T70486), and the University Professional Degree Postgraduate Research Practice Program of Jiangsu Province (NOs. SJZZ-0136).

## References

[1] K. Li, Z. Zeng, L.S. Yan, S.L. Luo, Appl. Catal. B-Environ. 165 (2015) 428–437.
[2] Q. Li, N. Zhang, Y. Yang, G.Z. Wang, Langmuir 30 (2014) 8965–8972.
[3] R. Rahimi, H. Kerdari, M. Rabbani, Desalination 280 (2011) 412–418.
[4] M. Tahir, C.B. Cao, F. Butt, Chemistry 16 (2014) 1825–1830.
[5] N. Zhang, S.Q. Liu, Y.J. Xu, Nanoscale 4 (2012) 2227–2238.
[6] Y.X. Zhu, Y.F. Wang, Z. Chen, Appl. Catal. A-Gen. 498 (2015) 159–166.
[7] J. Wang, X. Ni, Solid. State Commun. 146 (2008) 239–244.
[8] E. Moghaddam, A. Kazemzadeh, Appl. Surf. Sci. 346 (2015) 111–114.
[9] Y.G. Xu, H. Xu, L. Wang, J. Yan, Dalton Trans. 42 (2013) 7604–7613.
[10] D.M. Chen, K.W. Wang, Appl. Catal. B-Environ. 166–167 (2015) 366–373.
[11] M. Tahir, C. Cao, N. Mahmood, F.K. Butt, A. Mahmood, ACS Appl. Mater. Interfaces 6 (2014) 1258–1265.
[12] K. Katsumata, R. Motoyoshi, N. Matsushita, K. Okada, J. Hazard. Mater. 260 (2013) 475–482.
[13] K. Srinivasu, B. Modak, S. Ghosh, J. Phys. Chem. C 118 (2014) 26479–26484.
[14] D.J. Martin, P.J. Reardon, J. Am. Chem. Soc. 136 (2014) 12568–12571.
[15] M. Tahir, C.Cao Faheem, F. Idrees, Z. Ali, Cryst. Eng. Comm. 16 (2014) 1825–1830.
[16] X.J. Bai, S.C. Yan, J.J. Wang, J. Mater. Chem. A 2 (2014) 17521–17529.
[17] Y. Wang, J.H. Zhang, X.C. Wang, M. Antonietti, Angew. Chem. Int. Ed. 49 (2010) 3356–3359.
[18] X.X. Wang, S.S. Wang, W.D. Hu, J. Cai, Mater. Lett. 115 (2014) 53–56.
[19] J.S. Zhang, M.W. Zhang, S. Lin, J. Catal. 310 (2014) 24–30.
[20] S.W. Hu, L.W. Yang, Y. Tian, App. Catal. B-Environ. 163 (2015) 611–622.
[21] X. Zhong, M.M. Jin, H.Q. Dong, J. Solid. State Chem. 220 (2014) 54–59.
[22] M.L. Lu, Z.X. Pei, Phys. Chem. Chem. Phys. 16 (2014) 21280–21288.
[23] X.S. Zhou, B. Jin, R.Q. Chen, Mater. Res. Bull. 48 (2013) 1447–1452.
[24] Z.Y. Lu, W.C. Zhou, P.W. Huo, Chem. Eng. J. 225 (2013) 34–42.
[25] Z. Zhu, Z.Y. Lu, X.X. Zhao, Y.S. Yan, W.D. Shi, RSC Adv. 5 (2015) 40726–40736.
[26] W.J. Chen, P.J. Tsai, Y.C. Chen, Small 4 (2008) 485–491.
[27] G. Xi, B. Yue, J. Cao, J. Ye, Chem-Eur. J. 17 (2011) 5145–5154.
[28] L. Ren, S. Huang, W. Fan, T. Liu, Appl. Surf. Sci. 258 (2011) 1132–1138.
[29] S.K. Park, T. Ishikawa, Y. Tokura, Phys. Rev. B 58 (1998) 3717–3720.
[30] S. Kumar, T. Surendar, B. Kumar, A. Baruah, J. Phys. Chem. C 117 (2013) 26135–26143.
[31] Y.X. Tang, V.P. Subramaniam, D.G. Gong, Appl. Catal. B-Environ. 106 (2011) 577–585.
[32] M.S. Zhu, P.L. Chen, M.H. Liu, ACS Nano 5 (2011) 4529–4536.
[33] X. Dai, M.L. Xie, S.G. Meng, Appl. Catal. B-Environ. 158–159 (2014) 382–390.
[34] H.Y. Zhang, A.C. Yu, J. Phys. Chem. C 118 (2014) 11628–11635.
[35] T. Zhou, Y.G. Xu, H. Xu, Ceram. Int. 40 (2014) 9293–9301.
[36] J.S. Zhang, M.W. Zhang, C. Yang, Adv. Mater. 26 (2014) 4121–4126.
[37] C. Hu, T.W. Peng, X.X. Hu, Y.L. Nie, J. Am. Chem. Soc. 132 (2010) 857–862.
[38] P. Wang, B.B. Huang, X.Y. Qin, Angew. Chem. Int. Ed. 47 (2008) 7931–7933.
[39] L. Ge, C.C. Han, J. Liu, Appl. Catal. A-Gen. 409–410 (2011) 215–222.
[40] Y.M. He, L.H. Zhang, et al., Environ. Sci. Technol. 49 (2015) 649–656.
[41] Z.Y. Lu, F. Chen, M. He, Chem. Eng. J. 249 (2014) 15–26.
[42] X.J. Bai, R.L. Zong, C.X. Li, D. Liu, Appl. Catal. B-Environ. 147 (2014) 82–91.
[43] K.X. Li, Z.X. Zeng, L.S. Yan, Appl. Catal. B-Environ. 165 (2015) 428–437.
[44] Y.S. Jun, E.Z. Lee, X.C. Wang, Adv. Funct. Mater. 583 (2013) 3661–3667.
[45] Q.J. Xiang, J.G. Yu, M.J. Phys, Chem. C 115 (2011) 7355–7363.
[46] J.Z. Jiang, L. Ou-yang, L.H. Zhu, Carbon 80 (2014) 213–221.
[47] A. Roychowdhury, S.P. Pati, S. Kumar, D. Das, Mater. Chem. Phys. 151 (2015) 105–111.
[48] J.Z. Wang, G.H. Zhao, Y.F. Li, Dalton. Trans. 43 (2014) 11637–11645.
[49] Q. Liu, Y.M. Zheng, L.B. Zhong, J. Environ. Sci-China 28 (2015) 29–36.
[50] H.J. Dong, G. Chen, J.X. Sun, Appl. Catal. B-Environ. 134–135 (2013) 46–54.
[51] H.J. Dong, G. Chen, J.X. Sun, Chem. Commun. 50 (2014) 6596–6599.
[52] J.H. Liu, Y.W. Zhang, L.H. Lu, Chem. Commun. 48 (2012) 8826–8828.
[53] Y.J. Wang, X.J. Bai, X.C. Pan, J. He, Y. Zhu, J. Mater. Chem. 22 (2012) 11568–11573.
[54] H.H. Yin, K. Yu, C.Q. Song, A.C.S. Appl, Mater. Interfaces 6 (2014) 14851–14860.
[55] S. Fang, K.L. Lv, Q. Li, H.P. Ye, D.Y. Du, M. Li, Appl. Surf. Sci. (2015), http://dx.doi.org/10.1016/j.apsusc.201507179.
[56] K.L. Lv, J.C. Hu, X.H. Li, M. Li, J. Mol. Catal. A 356 (2012) 78–84.
[57] Y.J. Lin, S. Zhou, X.H. Liu, S. Sheehan, J. Am. Chem. Soc. 131 (2009) 2772–2773.
[58] Z.A. Huang, Q. Sun, K.L. Lv, Z.H. Zhang, M. Li, B. Li, Appl. Catal. B-Environ. 164 (2015) 420–427.
[59] D. Wang, H.T. Sun, Q.Z. Luo, X.L. Yang, Appl. Catal. B-Environ. 156–157 (2014) 323–330.
[60] W.J. Li, D.Z. Li, Y.M. Lin, J. Phys. Chem. C 116 (2012) 3552–3560.
[61] Y.P. Liu, L. Lu Fang, L.J. Liu, H. Wang, Catal. Commun. 17 (2012) 200–204.